

Quantum Monte Carlo Study of Hole Binding and Pairing Correlations in the Three-Band Hubbard Model

M. Guerrero and J. E. Gubernatis

Theoretical Division, Los Alamos National Laboratory, Los Alamos, NM 87545

Shiwei Zhang

Department of Physics and Department of Applied Science

College of William and Mary, Williamsburg, VA 23187

(March 24, 2022)

Abstract

We simulated the 3-band Hubbard model using the Constrained Path Monte Carlo (CPMC) method in search for a possible superconducting ground state. The CPMC is a ground state method which is free of the exponential scaling of computing time with system size. We calculated the binding energy of a pair of holes for systems up to 6×4 unit cells. We also studied the pairing correlation functions versus distance for both the d-wave and extended s-wave channels in systems up to 6×6 . We found that holes bind for a wide range of parameters and that the binding increased as the system size is increased. However, the pairing correlation functions decay quickly with distance. For the extended s channel, we found that as the Coulomb interaction U_d on the Cu sites is increased, the long-range part of the correlation functions is suppressed and fluctuates around zero. For the $d_{x^2-y^2}$ channel, we found that the correlations decay rapidly with distance towards a small positive value. However, this value becomes smaller as the interaction U_d or the system size is increased.

I. INTRODUCTION

The discovery of high temperature superconductivity in copper oxide materials generated considerable effort to find simple electronic models that exhibit a superconducting phase. Since the mechanism for superconductivity is believed to lie within the CuO_2 planes, a variety of two-dimensional models have been proposed, the three principal ones being the (one-band) Hubbard, three-band Hubbard, and t-J models. Unfortunately, conclusive evidence for a superconducting phase has not been found in any of these models.¹

In this paper, we will report the results of a quantum Monte Carlo (QMC) study of the three-band Hubbard model. Of the three models, it has been less intensively studied, partially because of the general belief that its low energy excitation spectrum is similar to the other two. Indeed in the strong coupling limit, both the one-band and three-band Hubbard models have the t-J model as an approximate limit. However, there still remains some controversy on whether one-band models, like the Hubbard and t-J models, are adequate to describe the low energy physical properties of the cuprate superconductors. One of our objectives is to study the possible existence of superconductivity in the three-band model in regions where model parameters are physical as opposed to regions where asymptotic models are clearly more appropriate.

The most solid information about possible superconductivity in the one-band Hubbard model has come from a series of QMC calculations. For instance, using a finite temperature QMC method, White et al.² studied possible superconductivity in the Hubbard model. They found an attractive effective pairing interaction in the $d_{x^2-y^2}$ and extended s-wave channels. Moreo and Scalapino³ subsequently found pairing correlations but also found that they did not increase when the lattice size was increased. Their result, suggesting the absence of long range order, was consistent with an earlier QMC study by Imada and Hatsugai.⁴

The results of almost all QMC calculations of the Hubbard model however, are limited

by the fermion sign problem to high temperatures and small system sizes. These limitations had left open the possibility that superconductivity still lurked at larger systems and lower temperatures. Recently, a new QMC method, the Constrained Path Monte Carlo (CPMC) method,⁵ was developed to get around the sign problem. Using this method, Zhang et al.⁶ calculated ground-state pairing correlation functions for the Hubbard model as a function of the distance and found that as the system size or the interaction strength is increased the magnitude of the long-range part of the pairing correlation functions vanished for both the $d_{x^2-y^2}$ and extended s-wave channels. Although this method produces a variational solution, its results, together with the null results from previous QMC studies, are very discouraging for finding superconductivity in the one-band Hubbard model.

Past numerical work on the three-band model, has been less definitive about the existence of superconductivity. The work has mainly consisted of exact diagonalization computations⁷⁻⁹, where calculations of hole binding energies was emphasized, and QMC computations¹⁰⁻¹⁵ where magnetic and pairing calculations were emphasized. The exact diagonalization studies unequivocally established that holes can bind. In a number of cases binding only occurred for unphysical parameter ranges, and because of small systems sizes, the existence and symmetry of the pairing was difficult to access. The QMC studies, probably even more limited by the sign problem than those for the one-band model, established the existence of an extended s-wave and $d_{x^2-y^2}$ wave attractive pairing interaction. However, none of these QMC studies reported the behavior of the pairing correlation functions at large distances, which is the relevant quantity to establish the existence of long range order.

In the work reported here, we removed the limitations caused by the sign problem by applying the CPMC method to the three-band Hubbard model. We computed the binding energy for holes near half-filling for systems up to 6×4 unit cells. We found a wide range of physically relevant parameters for which the holes bind. As will be reported in more detail, we found that larger systems in fact make hole binding easier. We also find that the inclusion of the nearest neighbors Coulomb repulsion V_{pd} is not necessary for binding as was concluded in several of the exact diagonalization studies. For similar systems sizes

as the previous simulations, but at zero temperature, we looked at the pairing correlation functions *as a function of distance* and found that the pairing correlation functions decay quickly with distance and are suppressed with increasing lattice size and U_d . The extended s-wave channel is much more strongly suppressed than the $d_{x^2-y^2}$ channel. These trends are similar to those found in QMC simulations of the one-band model.

The remainder of our report is organized as follows: in Section II we define the Hamiltonian and the physical quantities calculated and discuss the choice of model parameters. In Section III we briefly describe the CPMC method, and then in Section IV we present the results for both the binding energy for holes and the pairing correlation functions. Finally in Section V, we discuss in detail our main conclusions.

II. THREE-BAND HUBBARD HAMILTONIAN

As proposed by Emery,¹⁶ the three-band model physically mimics the CuO_2 layer by having one Cu and two O atoms per unit cell, with the Cu atoms arranged on a square lattice and the O atoms centered on the edges of the square unit cells. In this layer, Emery assumed that the relevant orbitals are just those of copper $3d_{x^2-y^2}$ and oxygen $2p_x$ and $2p_y$.

The Hamiltonian has the form:

$$\begin{aligned}
H = & \sum_{\langle j,k \rangle \sigma} t_{pp}^{jk} (p_{j\sigma}^\dagger p_{k\sigma} + p_{k\sigma}^\dagger p_{j\sigma}) + \epsilon_p \sum_{j\sigma} n_{j\sigma}^p + U_p \sum_j n_{j\uparrow}^p n_{j\downarrow}^p \\
& + \epsilon_d \sum_{i\sigma} n_{i\sigma}^d + U_d \sum_i n_{i\uparrow}^d n_{i\downarrow}^d \\
& + V_{pd} \sum_{\langle i,j \rangle} n_i^d n_j^p + \sum_{\langle i,j \rangle \sigma} t_{pd}^{ij} (d_{i\sigma}^\dagger p_{j\sigma} + p_{j\sigma}^\dagger d_{i\sigma})
\end{aligned} \tag{1}$$

In writing the Hamiltonian, we adopted the convention that the operator $d_{i,\sigma}^\dagger$ creates a *hole* at a Cu $3d_{x^2-y^2}$ orbital and $p_{j,\sigma}^\dagger$ creates a *hole* in an O $2p_x$ or $2p_y$ orbital. U_d and U_p are the Coulomb repulsions at the Cu and O sites respectively, ϵ_d and ϵ_p are the corresponding orbital energies, and V_{pd} is the nearest neighbor Coulomb repulsion. As written, the model has a Cu-O hybridization $t_{pd}^{ij} = \pm t_{pd}$ with the minus sign occurring $j = i + \hat{x}/2$ and $j = i - \hat{y}/2$

and also hybridization $t_{pp}^{jk} = \pm t_{pp}$ between oxygen sites with the minus sign occurring for $k = j - \hat{x}/2 - \hat{y}/2$ and $k = j + \hat{x}/2 + \hat{y}/2$. These phase conventions are illustrated in Fig. 1.

The system is said to be half-filled when there is one hole per Cu site. At half-filling, for a wide range of parameters, its ground-state is an anti-ferromagnetic insulator just like the one-band Hubbard model. Its insulating gap, however, is a charge transfer one in contrast with the gap in the one-band model which is a Mott-Hubbard gap.

The values of the parameters in the Hamiltonian have been estimated by a number of different constrained density functional and quantum cluster calculations.^{17–20} Taken together, these estimates define a reasonably limited range of the parameters for which the model might be labeled as “physical.” We use Table I of Ref 20, which summarizes results from density functional and cluster calculations, as the principal guideline for the parameter range we explored.

The Cu site Coulomb repulsion U_d is large, making doubly occupancy of Cu sites by two holes very unfavorable. The next largest parameter, the charge transfer energy $\epsilon = \epsilon_p - \epsilon_d > 0$, plays a special role. Depending on the relative values of ϵ , U_d and the bandwidth W the system can be classified in different regimes.²¹ Estimates place the cuprate superconductors in the charge transfer regime, in which $W < \epsilon < U_d$. The remaining parameters are relatively comparable in magnitude. The role of the Cu-O hybridization t_{pd} is also special. This hybridization, through the super-exchange mechanism, generates an anti-ferromagnetic exchange interaction between the spins in the Cu sites.

If $\epsilon \gg U_d$, the three-band model maps into a one-band model with $t_{eff} \sim t_{pd}^2/\epsilon$ and $U = U_d$. For $U_d \gg t_{eff}$, the one-band model can in turn be mapped into the t-J model with $J = 4t_{eff}^2/U_d$. Zhang and Rice²² have argued that the t-J model can also be appropriate when $t_{pd} \ll \epsilon, U_d, U_d - \epsilon$ and $\epsilon < U_d$. In real materials, ϵ/t_{pd} is estimated to be $\sim 2.7 - 3.7$.²⁰ Therefore, besides the lack of conclusive evidence that the one-band model superconducts, it is also unclear that the mapping among the most studied models is appropriate for physical values of the parameters. In this paper we will examine the three-band model in the estimated range of parameters to detail the behavior of the model in its own right.

In what follows we scale all the energies by t_{pd} . We take $V_{pd} = 0$ since it is small ($V_{pd} \leq 0.8t_{pd}$ ¹⁹). This assumption simplifies the numerical algorithm significantly and reduces the computational time by at least a factor of four.

With the numerical method used, a variety of expectation values can be computed. We focused on two key quantities: the binding energy for doped holes and the pairing correlation functions as a function of the distance. The binding energy is defined as:

$$\Delta = (E_2 - E_0) - 2(E_1 - E_0) \quad (2)$$

with E_n the ground-state energy for n doped holes, where E_0 corresponds to the undoped (half-filled) case. If negative, this parameter indicates that it costs less to dope a second hole in the vicinity of the first hole than it does to create two isolated holes. In the thermodynamic limit Δ is expected to be the binding energy of a Copper pair. We calculated Δ for systems with 2×2 , 4×2 and 6×4 unit cells. We are unaware of any previous quantum Monte Carlo calculations of binding energy for the three-band model.

We also computed the extended s-wave and the $d_{x^2-y^2}$ pairing correlation functions:

$$P_\alpha(R) = \langle \Delta_\alpha^\dagger(R) \Delta_\alpha(0) \rangle \quad (3)$$

where

$$\begin{aligned} \Delta_\alpha(R) = \sum_{\vec{\delta}} f_\alpha(\vec{\delta}) \{ & [d_{\vec{R}\uparrow} d_{\vec{R}+\vec{\delta}\downarrow} - d_{\vec{R}\downarrow} d_{\vec{R}+\vec{\delta}\uparrow}] \\ & + [p_{\vec{R}\uparrow}^x p_{\vec{R}+\vec{\delta}\downarrow}^x - p_{\vec{R}\downarrow}^x p_{\vec{R}+\vec{\delta}\uparrow}^x] + [p_{\vec{R}\uparrow}^y p_{\vec{R}+\vec{\delta}\downarrow}^y - p_{\vec{R}\downarrow}^y p_{\vec{R}+\vec{\delta}\uparrow}^y] \} \end{aligned} \quad (4)$$

with $\vec{\delta} = \pm\hat{x}, \pm\hat{y}$. For extended s-wave pairing $f_{s^*}(\vec{\delta}) = 1$ for all $\vec{\delta}$ and for the $d_{x^2-y^2}$ pairing, $f_d(\vec{\delta}) = 1$ for $\vec{\delta} = \pm\hat{x}$ and $f_d(\vec{\delta}) = -1$ for $\vec{\delta} = \pm\hat{y}$. Here R denotes the distance between unit cells (taken from copper ion to copper ion). We will directly report these correlations functions as a function of R . We will not report its $q = 0$ spatial Fourier transformation and partial sums like $S_\alpha(L) = \sum_{R \leq L} P_\alpha(R)$ as it has been done in previous works¹⁰⁻¹⁵, because the magnitude of these quantities are dominated by a large peak in $P_\alpha(R)$ when R is less than a few nearest neighbor distances. Over these distances, P_α measures local

correlations among spin and charge fluctuations and has little information about long-range pairing correlations. In certain cases, we will also report the “vertex contribution” to the correlation functions (see, for example, White et. al²) defined as follows:

$$V_\alpha(R) = P_\alpha(R) - \bar{P}_\alpha(R) \quad (5)$$

where $\bar{P}_\alpha(R)$ is the contribution of two dressed non-interacting propagators. For each term in $P_\alpha(R)$ of the form $\langle c_{\uparrow}^\dagger c_{\uparrow} c_{\downarrow}^\dagger c_{\downarrow} \rangle$, $\bar{P}_\alpha(R)$ has a term like $\langle c_{\uparrow}^\dagger c_{\uparrow} \rangle \langle c_{\downarrow}^\dagger c_{\downarrow} \rangle$. We find that the conclusions remain the same no matter which quantity we look at.

III. CONSTRAINED PATH QUANTUM MONTE CARLO TECHNIQUE

Our numerical method is extensively described and benchmarked elsewhere.⁵ Here we only discuss its basic approximation. In the CPMC method, the ground-state wave function $|\Psi_0\rangle$ is projected from a known initial wave function $|\Psi_T\rangle$ by a branching random walk in an over-complete space of Slater determinants $|\phi\rangle$. In such a space, we can write $|\Psi_0\rangle = \sum_\phi \chi(\phi) |\phi\rangle$. The random walk produces an ensemble of $|\phi\rangle$, called random walkers, which represent $|\Psi_0\rangle$ in the sense that their distribution is a Monte Carlo sampling of $\chi(\phi)$, that is, a sampling of the ground-state wave function.

To completely specify the ground-state wave function, only determinants satisfying $\langle \Psi_0 | \phi \rangle > 0$ are needed because $|\Psi_0\rangle$ resides in either of two degenerate halves of the Slater determinant space, separated by a nodal plane \mathcal{N} that is defined by $\langle \Psi_0 | \phi \rangle = 0$. The sign problem occurs because walkers can cross \mathcal{N} as their orbitals evolve continuously in the random walk. Asymptotically they populate the two halves equally, leading to an ensemble that has zero overlap with $|\Psi_0\rangle$. If \mathcal{N} were known, we would simply constrain the random walk to one half of the space and obtain an exact solution of Schrödinger’s equation. In the constrained-path QMC method, without *a priori* knowledge of \mathcal{N} , we use a trial wave function $|\Psi_T\rangle$ and require $\langle \Psi_T | \phi \rangle > 0$. The random walk again solves Schrödinger’s equation in determinant space, but under an approximate boundary-condition. This is what is called the constrained-path approximation.

The ground-state energy computed by the CPMC method is an upper bound. The quality of the calculation clearly depends on the trial wave function $|\Psi_T\rangle$. Since the constraint only involves the overall sign of its overlap with any determinant $|\phi\rangle$, it seems reasonable to expect the results to show some insensitivity to $|\Psi_T\rangle$. Through extensive benchmarking on the Hubbard model, it has been found that simple choices of this function can give very good results.⁵

Besides as starting point and as a condition constraining a random walker, we also use $|\Psi_T\rangle$ as an importance function. Specifically we use $\langle\Psi_T|\phi\rangle$ to bias the random walk into those parts of Slater determinant space that have a large overlap with the trial state. For all three uses of $|\Psi_T\rangle$, it clearly is advantageous to have $|\Psi_T\rangle$ approximate $|\Psi_0\rangle$ as closely as possible. Only in the constraining of the path does $|\Psi_T\rangle \neq |\Psi_0\rangle$ generate an approximation.

All the calculations reported here are done with periodic boundary conditions. Mostly, we study closed shell cases, for which the corresponding free-electron wave function is non-degenerate and is translationally invariant. In these cases, the free-electron wave function, represented by a single Slater determinant, is used as the trial wave function $|\psi_T\rangle$. (The use of an unrestricted Hartree-Fock wave function as $|\psi_T\rangle$ produced no significant improvement in the results).

However, to calculate the binding energy for holes, we need to study the half filled case and then the 1 and 2 hole doped cases. In the systems considered (2×2 , 4×2 and 6×4 unit cells) the 2 hole doped case corresponds to a closed shell case. The one hole doped case is a closed shell minus one hole. This missing hole can be put in either of two degenerate orbitals corresponding to $\vec{k}_1 \equiv (0, \pi)$ or $\vec{k}_2 \equiv (\pi, 0)$. The trial wave function, constructed by putting the hole in either of these orbitals or a linear combination of them, give equally good results so we pick an arbitrary linear combination of them. For the half-filled case, the free electron wave function is 4-fold degenerate: $c_{k_1,\uparrow}^\dagger c_{k_1,\downarrow}^\dagger |CS\rangle$, $c_{k_2,\uparrow}^\dagger c_{k_2,\downarrow}^\dagger |CS\rangle$, $c_{k_1,\uparrow}^\dagger c_{k_2,\downarrow}^\dagger |CS\rangle$, $c_{k_2,\uparrow}^\dagger c_{k_1,\downarrow}^\dagger |CS\rangle$, where $|CS\rangle$ is the closed shell state with two holes below half-filling. In the 2×2 system the state $|CS\rangle$ has 2 holes, in the 4×2 system, it has 6 holes and in the 6×4 system it has 22 holes. If we just arbitrarily pick one of these states, the energy

has a significant difference. For example, in the 2×2 system it is of the order of 10^{-2} from the exact diagonalization result. To accurately compute the binding energy, this difference is too big. Therefore, we used the following procedure: we diagonalize the interacting part of the Hamiltonian in this degenerate subspace, and obtained 2 states with energy proportional to U_d and 2 states with zero energy. Of the 2 states with zero energy only one of them is a singlet. We used this state. It is represented by two Slater determinants: $(c_{k_1,\uparrow}^\dagger c_{k_1,\downarrow}^\dagger - c_{k_2,\uparrow}^\dagger c_{k_2,\downarrow}^\dagger)|CS > / \sqrt{2}$. In Table 1, for a 2×2 system with $\epsilon_p = 3$ and $U_p = t_{pp} = 0$, we compare the energies obtained using the CPMC with the one and two Slater determinants trial wave function and energies obtained from exact diagonalization. We see that using two Slater determinants improves the accuracy by an order of magnitude or more. The accuracy has become better than the closed shell case.

In a typical run for a large system we set the average number of walkers to 600 and the time step to 0.03. We perform 3000 steps before we start taking measurements and we do the measurements in 40 blocks of 500 steps each to ensure statistical independence.

IV. RESULTS

Shell structures are characteristic of finite-sized systems of electrons. In our simulations these effects are most clearly seen in the values of the energy and chemical potential as a function of the hole density $n = N_h/N$, with N the number of unit cells. A shell structure is perhaps most easily illustrated by first considering the non-interacting problem. There, holes are added to the system at the same energy until all the degenerate states of a given shell are occupied and paired, that is, until the shell is closed. As an “open” shell is filled, the total energy of the system varies linearly with the doping and within a shell the chemical potential thus is a constant. The number of states in a shell is twice the order of the point group relating the wave vectors of the degenerate states. Between shells the chemical potential is discontinuous. This “gap” is a finite size effect.

In the interacting problem the energy and chemical potential shows a similar behavior.

The number of states in a shell and the shell boundaries are the same as the non-interacting problem for the range of interactions we examined. For a 4×4 system, a typical shell structure for the three-band model as a function of U_d is illustrated in Figs. 2a and 2b where we show the ground state energy E_o and the chemical potential μ as a function of the hole density for $\epsilon = 3$, $t_{pp} = U_p = 0$. For our finite system we defined

$$\mu(N) = E_o(N) - E_o(N - 1) \quad (6)$$

which is the discrete version of the usual definition $\mu = \partial E_o / \partial N_h$. The $U_d = 0$ case is the non-interacting case. Its shell structure is most evident in the chemical potential, Fig. 2b. A comparison of the non-interacting case with the interacting cases does show several differences. At half-filling, $n = 1$, the chemical potential in the interacting cases shows a jump whereas the non-interacting case does not. This jump is not a finite-size effect but is the charge-transfer gap induced by the interaction. Within a shell the chemical potential of the interacting cases are varying weakly but approximately linearly with doping. This variation is similar to the behavior of the one-band Hubbard model^{23,24}, but there, to an excellent approximation, within a shell the energy for the interacting cases varies linearly with doping and hence within a shell the chemical potential is a constant. In Fig. 2a, one sees that the energy versus doping curve has a minimum whose location varies as a function of U_d . As U_d increases this location shifts from the fully doped position towards the half-filled position. The one-band Hubbard model displays similar doping and interaction dependencies.^{3,23,24}

A. Binding Energy for Holes

We calculated the binding energy Δ for holes for systems with 2×2 , 4×2 , and 6×4 unit cells. A value of $\Delta < 0$ indicates hole binding whereas a value of $\Delta > 0$ implies hole repulsion. It is important to note that studying systems larger than 2×2 is essential for the doping δ to have values similar to those for which the real materials superconduct: for

2×2 unit cells with one hole, $\delta = 0.25$, and with 2 holes, $\delta = 0.5$, values which are outside the physically interesting region. On the other hand, for one and two holes the 4×2 case has $\delta = 0.125$ and $\delta = 0.25$ while the 6×4 case has $\delta = 0.042$ and $\delta = 0.083$. These values of doping span the range observed in the real materials.

Shown in Fig. 3, to benchmark the accuracy of our results, is a comparison of our binding energies with those of exact diagonalization. Specifically, we plotted Δ as a function of U_d for 2×2 systems with $U_p = t_{pp} = 0$ and $\epsilon = 2$ and 3 and found good agreement with exact diagonalization results, especially for the $\epsilon = 2$ case. For $\epsilon = 3$ the differences are more pronounced but are still only of the order of 10^{-3} . As a general trend, we slightly *underestimate* the binding energy. This figure is representative of our systematic error in the estimation of the binding energy.

In Fig. 4 we present results for 4×2 systems as function of ϵ as function of two values of U_d . For $U_d = 1$ we find that Δ decreases monotonically with ϵ but for $U_d = 4$ it has a shallow minimum at $\epsilon \sim 2$. Such a minimum means that there is a broad range of ϵ for which the binding energy does not change significantly. The existence of such a minimum, occurring at approximately the same value of ϵ , was observed in the exact diagonalization studies of Ogata and Shiba⁷ and commented upon by Martin.²⁰ In general holes bind provided ϵ is below some threshold value. In what follows, we set $\epsilon = 3$ which is a value consistent with the values obtained by LDA and cluster calculations²⁰ and is also near the optimal value for binding.

In Fig. 5, we compare Δ for different systems sizes as a function of U_d . We find that the binding energy tends to saturate as U_d is increased. The saturation is consistent with the exact diagonalization studies of Ogata and Shiba⁷ and of Stephan et al.⁹ The binding energy tends to increase as the system size is increased. Over the range of system sizes studied, the dependence of Δ on system size was not systematic enough to allow us to extrapolate to infinite system sizes. In general $\Delta \sim 10^{-2}$.

We also studied the effect of U_p and t_{pp} on Δ . In Fig. 6 we plot Δ as a function of U_d for $U_p = 0$ and $U_p = 1$. In Fig. 6a, we see that in the 2×2 system a small value of U_p

destroys the binding as previously reported by Hirsch et al.⁸ However, in the larger 4×2 system (Fig. 6b), the holes still bind with $U_p = 1$, although the binding energy is smaller, confirming a speculation of Hirsch et al. that the negative effect of U_p on the binding might decrease as the system size increases. A similar effect is seen when we plot Δ versus t_{pp} for 2×2 and 4×2 systems with $U_d = 6$, $\epsilon = 3$ and $U_p = 0$ (Fig. 7). The ability to bind decreases nearly linearly with t_{pp} but in the larger systems it decreases more slowly, so that there is still binding for $t_{pp} = 0.3$. Therefore, the effect of the Coulomb repulsion on the O sites and hopping between them in reducing the binding is diminished for larger system sizes. In contrast to the position emphasized by Hirsch et al.⁸ and by Stephan et al.,⁹ the physical presence of a non-zero t_{pp} and U_p , while reducing the ability to bind, does not necessarily mean that an unphysically large Cu-O Coulomb repulsion V_{pd} is essential for hole binding. Their conclusions were influenced by the small system sizes they were able to study.

While the binding of two holes in the physically relevant range of parameters is encouraging for superconductivity, perhaps a more central question now is what happens when a third hole is added. Do the three holes cluster or does the third hole sit apart from the pair? We do not examine these questions directly. Instead, we calculate the superconducting pairing correlations.

B. Pairing Correlation Functions

For both the extended s-wave and the $d_{x^2-y^2}$ channels, we studied the pairing correlation functions as a function of the distance for lattices up to 6×6 unit cells. All calculations were done for closed shell cases. For the 4×4 systems, we put 18 holes ($\delta = 0.125$), for the 6×6 system, 42 holes ($\delta = 0.167$), and for 6×4 , 26 holes ($\delta = 0.083$). The distance is measured between unit cells (from copper ion to copper ion)²⁵.

In Fig. 8 we present the pairing correlations for the extended s-wave channel of a 6×6 system with $\epsilon = 3$ and $t_{pp} = 0.3$ for different values of the interaction U_d . The inset magnifies the large distance behavior. We see that the short-ranged correlations are enhanced with

increasing U_d , but decay very quickly when R is increased. For large R they simply fluctuate around 0. For the same parameters, the $d_{x^2-y^2}$ channel is plotted in Fig. 9. Again, there is enhancement in the short-ranged part. Then as R is increased, there is again a decay, in this case not to zero but to a small positive value. However, as U_d is increased, this value becomes even smaller. These results clarify the findings of previous quantum Monte Carlo simulations. These previous simulations were limited to relatively high temperatures because of the sign problem. Scalettar and coworkers¹¹ found an attractive pairing interaction in both the extended s and the $d_{x^2-y^2}$ channels but could not predict which would dominate with the lowering of temperature and increasing of lattice size. The results of Figs. 8 and 9 clearly indicate that the $d_{x^2-y^2}$ correlations dominate. This dominance is in direct opposition to the findings of Dopf and coworkers^{12,13} that the extended s wave channel dominates. By looking at the the zero wave number component of the Fourier transform of the pairing correlation function, these researchers only observed how the short-ranged correlations behaved and overshadowed the behavior of the longer-ranged correlations.

In several previous quantum Monte Carlo simulations various researchers found it more convenient to study just the vertex contribution to the pairing correlation function, as defined in section II. In Fig. 10 we plot this contribution to the $d_{x^2-y^2}$ correlation function just shown in Fig. 9. We see that there is positive contribution which again is enhanced by U_d at short distances but suppressed at larger distances. Thus, as emphasized by Zhang et al.,⁶ this function seems to contain no more information about possible long-range order than the full pairing correlation function.

Since we restricted ourselves to closed shell cases, it is difficult to do a useful finite-size scaling of our results. An attempt to show the effect of increasing system size on the correlations is given in Fig. 11 where we plot the $d_{x^2-y^2}$ vertex contribution for 4×4 and 6×6 systems with the same parameters, keeping in mind that the fillings are not the same. At short distances the correlations are enhanced as the lattice size is increased but for larger distances there is a crossover, and in fact, the vertex contribution is smaller in the 6×6 system by almost an order of magnitude. A similar significant reduction is also seen in the

long-range parts of the full correlation functions.

We also studied the effect of ϵ and t_{pp} on the pairing correlations. One will recall that increasing t_{pp} weakened pair binding while the binding was optimal for ϵ around 2. In Fig. 12 we plot the bare correlation functions for different values of ϵ with $U_d = 6$ and $t_{pp} = 0.3$ for a 6×4 system with $\delta = 0.083$. We find that the long-range pairing correlations are not optimal when the pair binding is optimal. In fact, values of ϵ less than the optimal value enhance the longer range part of the correlation functions. A much smaller effect is obtained by changing the value of t_{pp} , as evident in Fig. 13, where the parameters are $U_d = 6$, $\epsilon = 3$ and the size is 6×6 unit cells. If anything, the larger value of t_{pp} seems to enhance the long-range correlations slightly.

It is interesting that in all cases presented we see a crossover from what happens at short distances to what happens at long distances. We emphasize that examining quantities that integrate, even partially, the pairing correlation function over distances can produce misleading results.

V. SUMMARY AND CONCLUSIONS

Using a newly developed quantum Monte Carlo method, the constrained-path method, we simulated the 3-band Hubbard model to search for a possible superconducting ground state. We focused principally on the calculation of the binding energy of a pair of holes and the extended s and $d_{x^2-y^2}$ superconducting pairing correlation functions. For the pair binding energy, we found that holes bind for a wide physically relevant range of parameters and that the binding increased as the system size is increased. We also found that when we included a hopping t_{pp} between oxygen sites, the binding decreased roughly linearly with t_{pp} , but in a larger system it decreased much more slowly. The Coulomb repulsion U_p on the oxygen sites was found to suppress the binding, but again for larger systems its effect became less significant. The increased tendency to bind as the system size is increased seems to diminish the importance of an Cu-O Coulomb repulsion V_{pd} for holes to bind as suggested

in several exact diagonalization studies.^{8,9} In general, hole binding occurs over a broad range of ϵ values centered roughly around two. In this respect our simulations support the exact diagonalization results of Ogata and Shiba.⁷

We calculated the pairing correlation functions for the extended s and the $d_{x^2-y^2}$ channels as a function of the distance. For the extended s channel, we found that as the Coulomb interaction U_d on the Cu sites is increased, the long-range part of the correlation functions is suppressed and fluctuates around zero. For the $d_{x^2-y^2}$ channel, we found that the correlations decay rapidly with distance towards a small positive value. However, this value becomes smaller as the interaction U_d or the system size is increased. The same behavior is observed for the vertex contributions to these correlation functions. Unequivocally, the $d_{x^2-y^2}$ pairing correlations dominate the extended s pairing correlations. This finding is opposite to that previously emphasized by Dopf and coworkers.¹²⁻¹⁴

We also studied the effect of the charge transfer energy ϵ on the pairing correlation functions and found that smaller values of ϵ produce larger correlations. Similarly, we looked at the effect of the hopping t_{pp} between oxygen sites and found that it has a very small effect but that larger values of t_{pp} are slightly more favorable for pairing. These trends are counter to those that enhance pair binding.

A systematic study of the size dependence of the binding energy and pairing correlation functions was difficult because the way the doping dependence of closed shell changed with changing system sizes. We did present a comparison of the $d_{x^2-y^2}$ pairing correlation function for a 4×4 system and a 6×6 system. Although the hole doping was slightly different, a significant reduction of both the vertex contribution and the full correlation function was observed in the larger system. This result suggests that the long-range pairing correlation found are unlikely to persist in the thermodynamic limit.

In general, we found similar trends for the three-band model that were found for the one-band Hubbard model.⁶ The additional degrees of freedom in the three-band model do not seem to enhance superconductivity in an obvious way. One could argue that a Cu-O Coulomb repulsion V_{pd} is needed; however, we found that V_{pd} is not necessary to obtain hole

binding and speculate that it is unlikely that the addition of such a small parameter to the model would change the picture dramatically. The question remains, if the holes do bind, that is, a purely electronic mechanism induces an attractive interaction between holes, but this attraction does not lead to electron pairing, what does it, if anything, lead to. Does it lead to phase separation or some novel phase, like stripes? This question is currently under investigation.

ACKNOWLEDGMENTS

We are thankful to Tinka Gammel for providing exact diagonalization results. The C++ program used for this work incorporated the *MatrixRef* matrix classes written by S.R. White, available at <http://hedrock.ps.uci.edu>. We acknowledge many helpful discussions with J. Carlson, Richard L. Martin and B. H. Brandow.

REFERENCES

- ¹ See for example, Elbio Dagotto, Rev. Mod. Phys., **66**, 763 (1994).
- ² S. R. White, D. J. Scalapino, R. L. Sugar, N. E. Bickers, R. T. Scalettar, Phys. Rev. B, **39**, 839 (1989).
- ³ A. Moreo and D. J. Scalapino, Phys. Rev. B, **43**, 8211 (1991).
- ⁴ Masatoshi Imada and Yasuhiro Hatsugai, J. Phys. Soc. Jpn., **58**, 3752 (1989).
- ⁵ Shiwei Zhang, J. Carlson and J. E. Gubernatis, Phys. Rev. Lett., **74**, 3652 (1995); Phys. Rev. B, **55** 7464 (1997).
- ⁶ Shiwei Zhang, J. Carlson and J. E. Gubernatis, Phys. Rev. Lett., **78**, 4486 (1997).
- ⁷ Masao Ogata and Hiroyuki Shiba, J. Phys. Soc. Jpn., **57**, 3074 (1988).
- ⁸ J. E. Hirsch, S. Tang, E. Loh Jr., D. J. Scalapino, Phys. Rev. Lett., **60** 1668 (1988); Phys. Rev. B, **39** 243 (1989).
- ⁹ W. H. Stephan, W. v. d. Linden and P. Horsch, Phys. Rev. B, **39** 2924 (1989).
- ¹⁰ R. T. Scalettar, Physica C, **162-164**, 313 (1989).
- ¹¹ R. T. Scalettar, D. J. Scalapino, R. L. Sugar, S. R. White, Phys. Rev. B, **44**, 770 (1991).
- ¹² G. Dopf, A. Muramatsu, and W. Hanke, Phys. Rev. B, **41**, 9264 (1990).
- ¹³ G. Dopf, A. Muramatsu, and W. Hanke, Phys. Rev. Lett., **68**, 353 (1992).
- ¹⁴ G. Dopf, J. Wagner, P. Dieterich, A. Muramatsu, and W. Hanke, Helv. Phys. Acta **65**, 257 (1992).
- ¹⁵ Kazuhiko Kuroki and Hideo Aoki, Phys. Rev. Lett., **76**, 4400 (1996).
- ¹⁶ V. J. Emery, Phys. Rev. Lett., **58**, 2794 (1987).
- ¹⁷ M. S. Hybertsen, M. Schuluter and N. E. Christensen, Phys. Rev. B, **39**, 9028 (1989).

- ¹⁸ H. Eskes, G. A. Sawatzky, L. F. Feiner, *Physica C*, **160**, 424 (1989).
- ¹⁹ A. K. McMahan, J. F. Annet and R. M. Martin, *Phys. Rev. B*, **42**, 6268 (1990).
- ²⁰ Richard L. Martin, *Phys. Rev. B*, **53**, 15501 (1996).
- ²¹ J. Zaanen and A. M. Oleś, *Phys. Rev. B*, **37**, 9423 (1988).
- ²² F. C. Zhang and T. M. Rice, *Phys. Rev. B*, **37**, 3759 (1998).
- ²³ N. Furukawa and M. Imada, *J. Phys. Soc. Jpn.*, **61**, 3331 (1992).
- ²⁴ Shiwei Zhang, J. Carlson and J. E. Gubernatis, unpublished.
- ²⁵ There are cases where for a same distance R between unit cells but different orientations of the vector \vec{R} , the value of the correlation function is different. This occurs either due to the geometry of the unit cell or the fact that we used a rectangular lattice. In these cases we averaged the different values of the correlation functions.

TABLES

TABLE I. Comparison of the exact ground-state energy with the CPMC result with a one and two Slater determinant trial wave function for a 2×2 system. Parameters are $\epsilon = 3$ and $t_{pp} = U_p = 0$. The use of two Slater determinants as described in the text improves the accuracy by an order of magnitude or more.

U_d	CPMC 1SD	CPMC 2SD	Exact
1	-5.0613(3)	-5.0764(2)	-5.076977
2	-4.8475(9)	-4.8789(7)	-4.880047
4	-4.6073(9)	-4.6615(6)	-4.661723
6	-4.4884(9)	-4.5468(6)	-4.547436

FIGURES

FIG. 1. Phase convention for the hopping matrix elements. The copper $d_{x^2-y^2}$ orbital is surrounded by the oxygen p_x and p_y orbitals. The hopping matrix elements are shown with their corresponding phase.

FIG. 2. (a) Ground state energy per unit cell as a function of the hole density for a 4×4 system with $\epsilon = 3$, $t_{pp} = U_p = 0$. The energy decreases monotonically for $U_d = 0$ but goes through a minimum for $U_d > 0$. For large U_d the minimum appears at half-filling. (b) Chemical potential as a function of the hole density for the same parameters. The shell structure is evident. For large U_d a charge transfer gap appears at half-filling.

FIG. 3. Comparison of the binding energy as a function of U_d with exact diagonalization results for 2×2 systems with $t_{pp} = U_p = 0$ and $\epsilon = 2$ and 3. Our results are in reasonable good agreement with the exact ones.

FIG. 4. Binding energy Δ as a function of ϵ for a 4×2 system with $t_{pp} = U_p = 0$. For $U_d = 1$ it decreases monotonically but for $U_d = 4$ it has a shallow minimum near $\epsilon \sim 2$.

FIG. 5. Binding energy Δ as a function of U_d for different system sizes with $\epsilon = 3$ and $t_{pp} = U_p = 0$. The binding increases as the system size is increased.

FIG. 6. Effect of U_p on the binding energy, $\epsilon = 3$ and $t_{pp} = 0$. (a) In the 2×2 system the binding disappears completely for $U_p = 1$. (b) In the 4×2 system the binding is still present for $U_p = 1$ although is slightly suppressed.

FIG. 7. Effect of t_{pp} on the binding energy for 2×2 and 4×2 systems with $\epsilon = 3$, $U_d = 6$ and $U_p = 0$. The binding energy decreases roughly linearly with t_{pp} but it decreases much more slowly in the larger system.

FIG. 8. Extended s-wave pairing correlation functions vs. distance for different values of U_d for a 6×6 system with $\epsilon = 3$ and $t_{pp} = 0.3$. The correlations decay rapidly and oscillate around zero at larger distances.

FIG. 9. d-wave pairing correlation functions vs. distance for different values of U_d with the same parameters as in Fig. 8. The correlations decay towards a small positive value at large distances.

FIG. 10. Vertex contribution for the d-wave pairing correlation functions vs. distance for the same parameters as in Fig. 8. It converges to a small value at large distances and this value decreases as U_d increases.

FIG. 11. Comparison of the vertex contribution for the d-wave pairing correlations for two different system sizes with $U_d = 6$, $\epsilon = 3$ and $t_{pp} = 0.3$. Although the fillings are slightly different in each case, a strong reduction is seen in the larger system.

FIG. 12. d-wave pairing correlation functions for different values of ϵ with $U_d = 6$, $U_p = t_{pp} = 0$ for a 6×4 system with $\delta = 0.083$. The smaller values of ϵ are more favorable for pairing.

FIG. 13. Effect of t_{pp} on the d-wave pairing correlation functions in a 6×6 system with $U_d = 6$ and $\epsilon = 3$. A very small increase is seen as t_{pp} is increased.

Figure 1

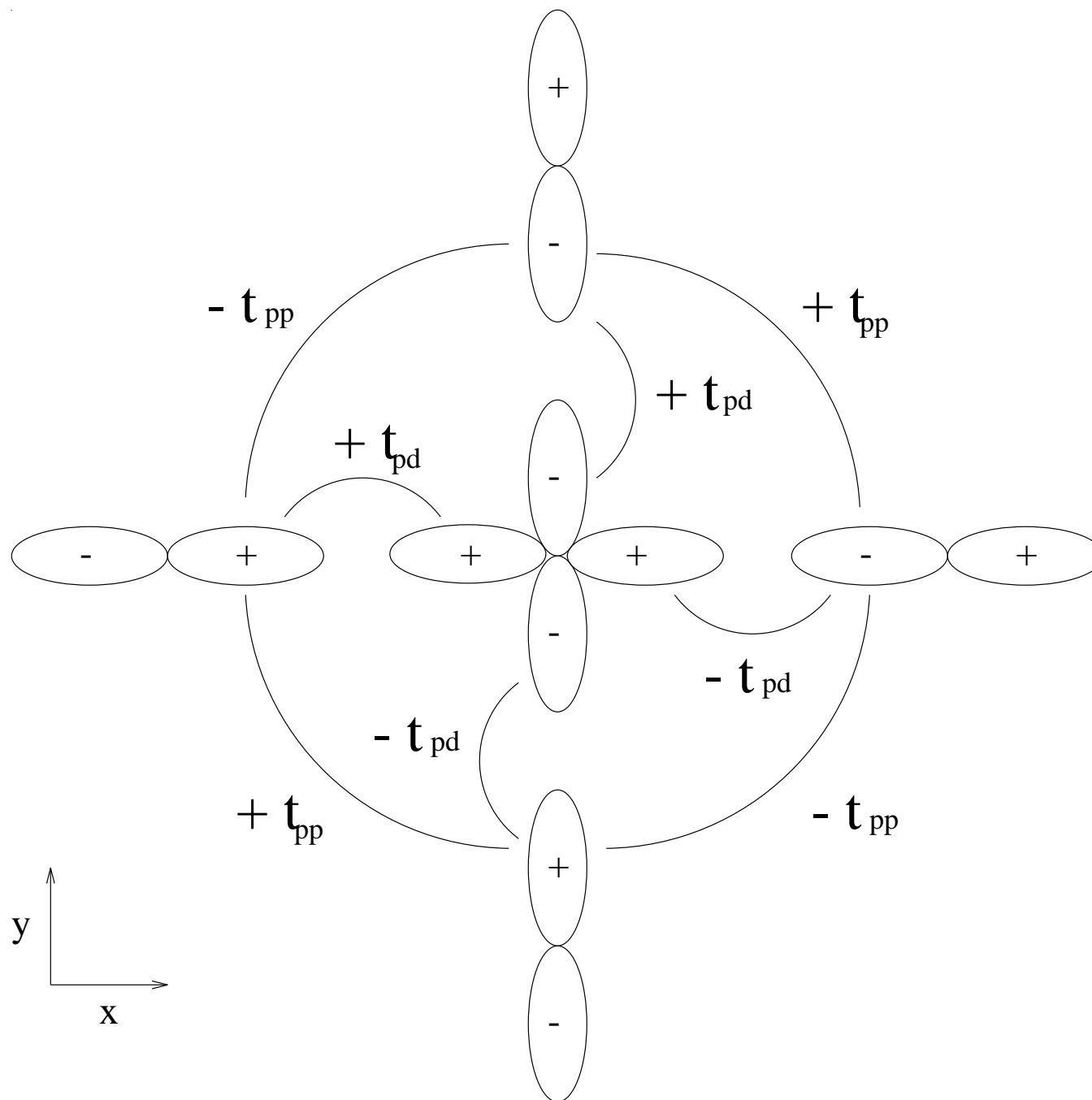


Figure 2a

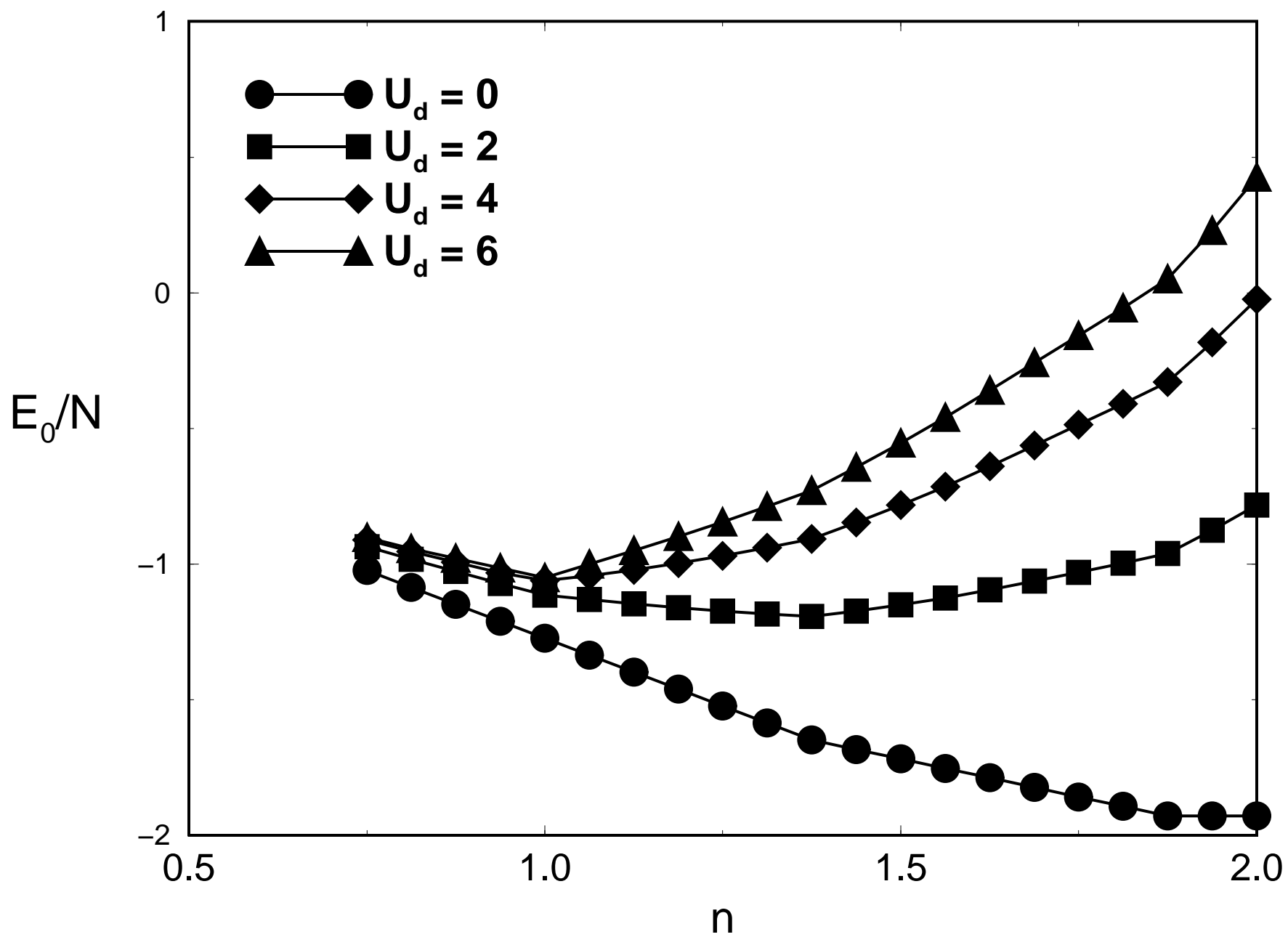


Figure 2b

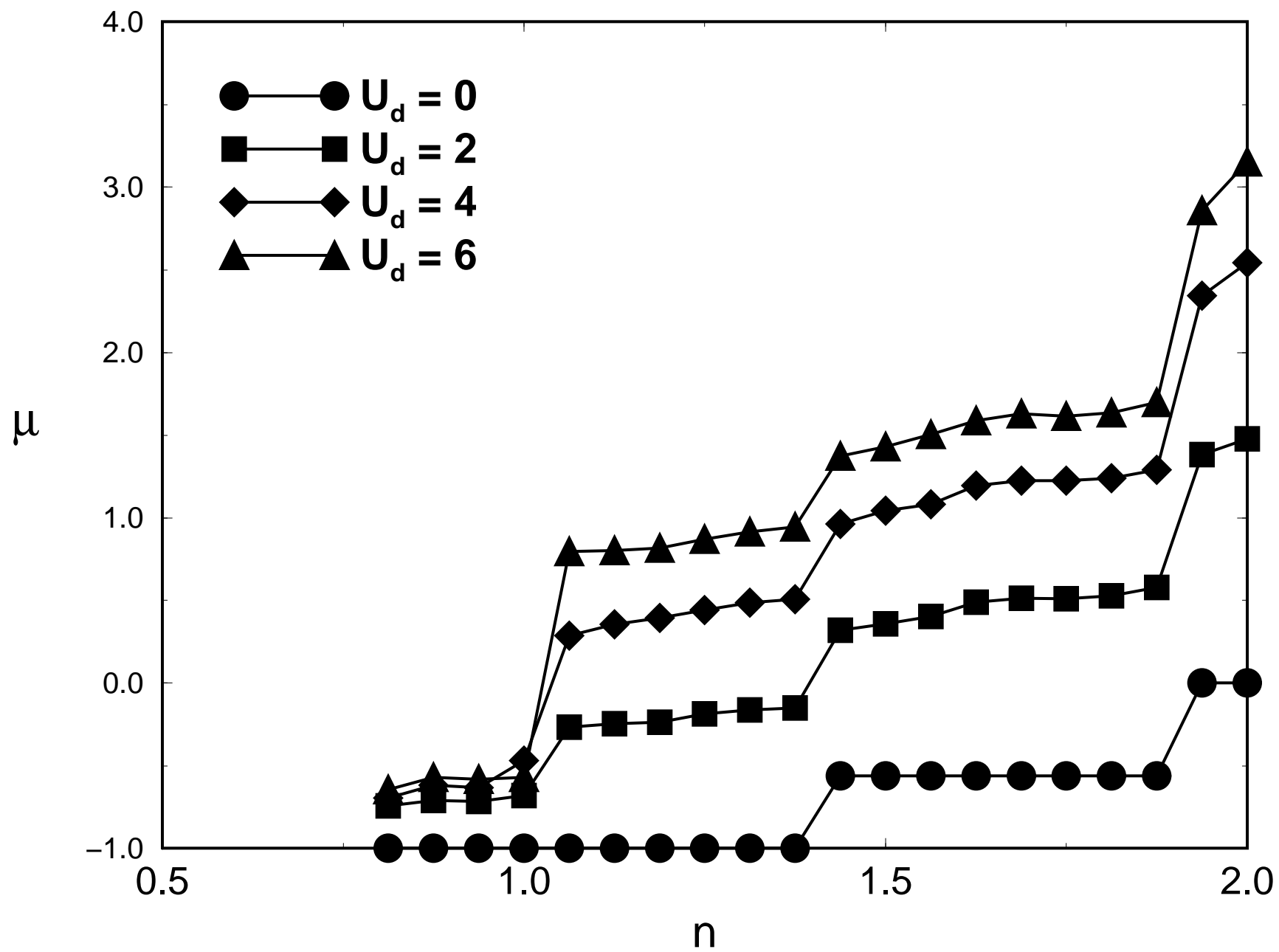


Figure 3

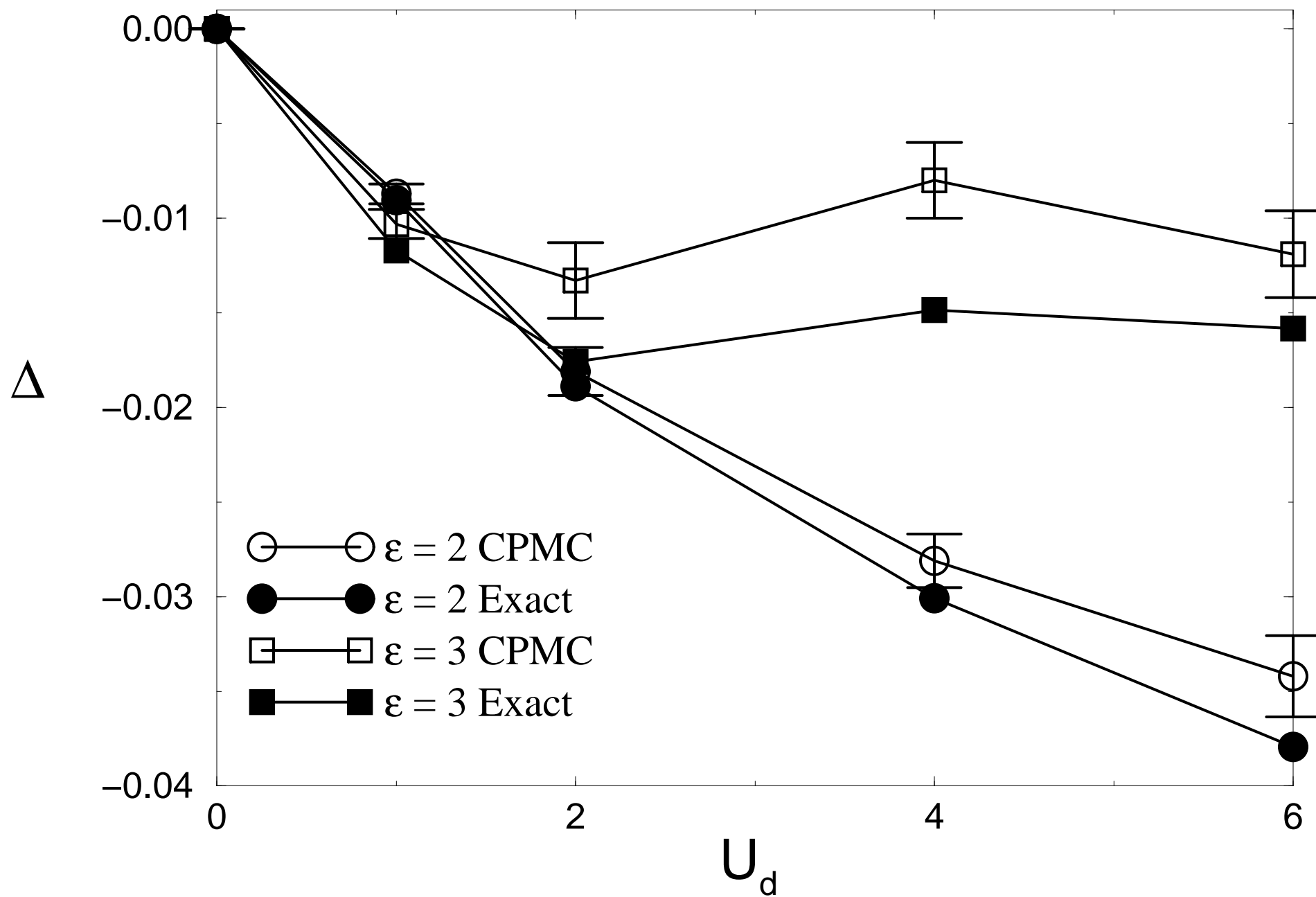


Figure 4

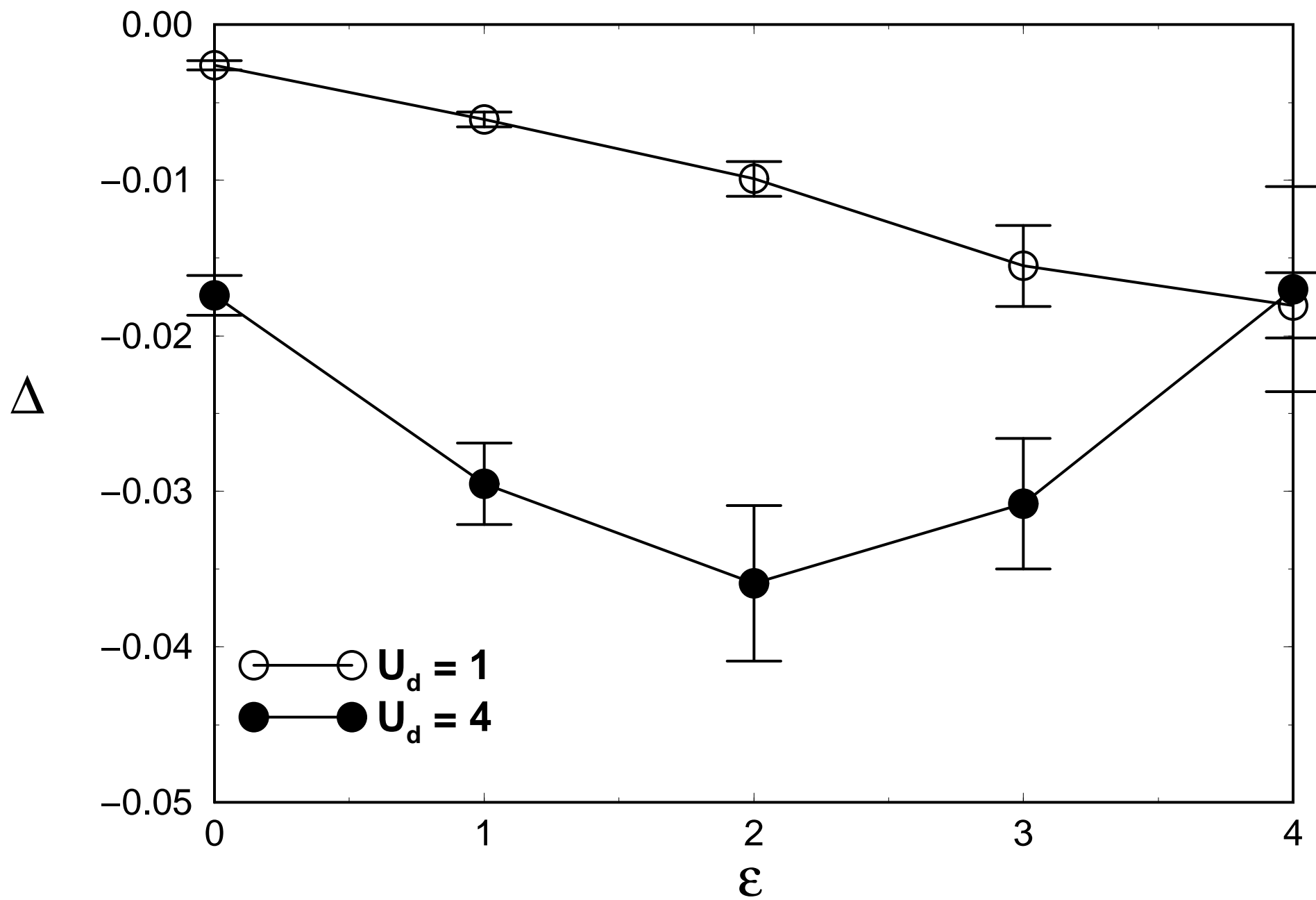


Figure 5

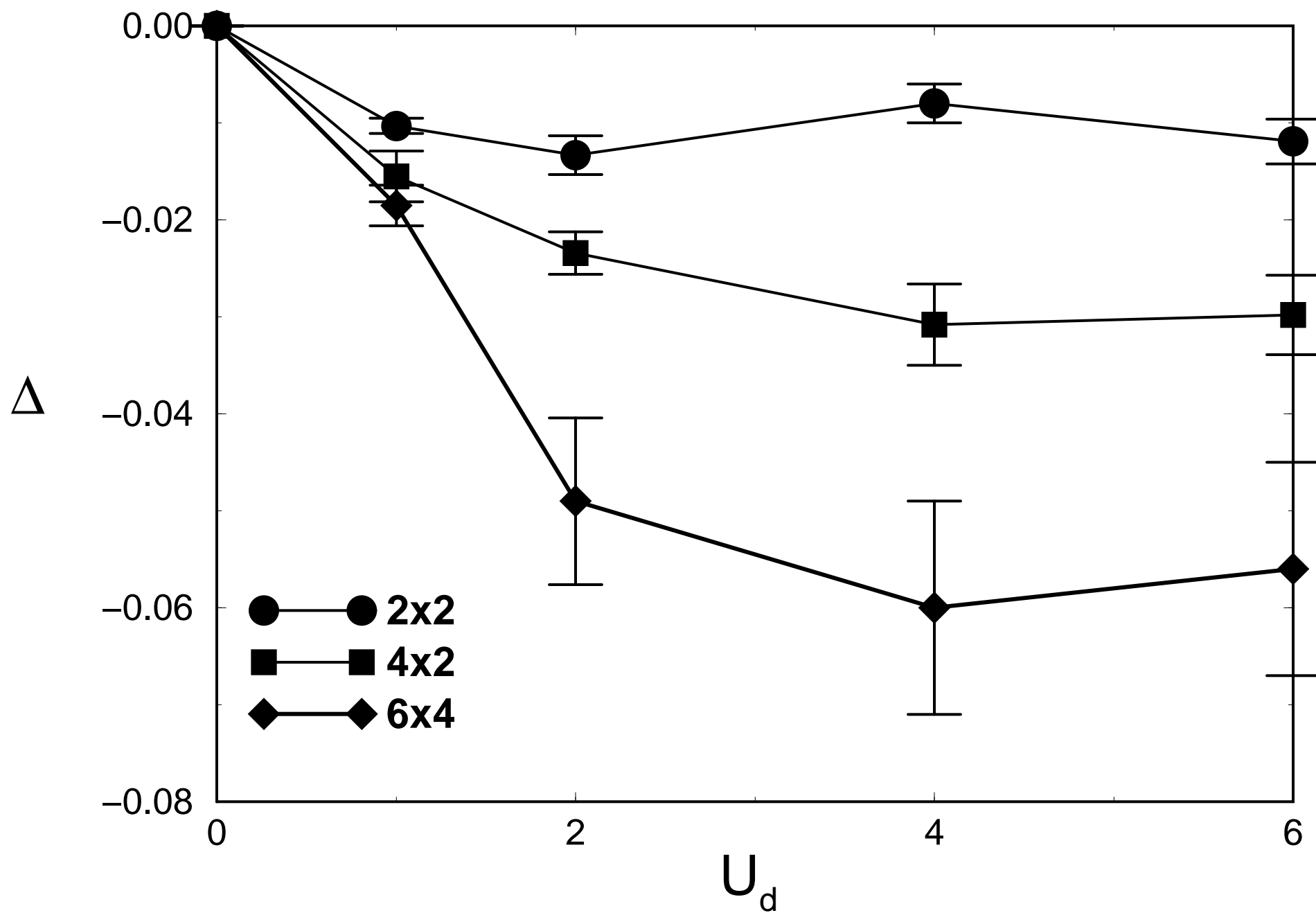


Figure 6a

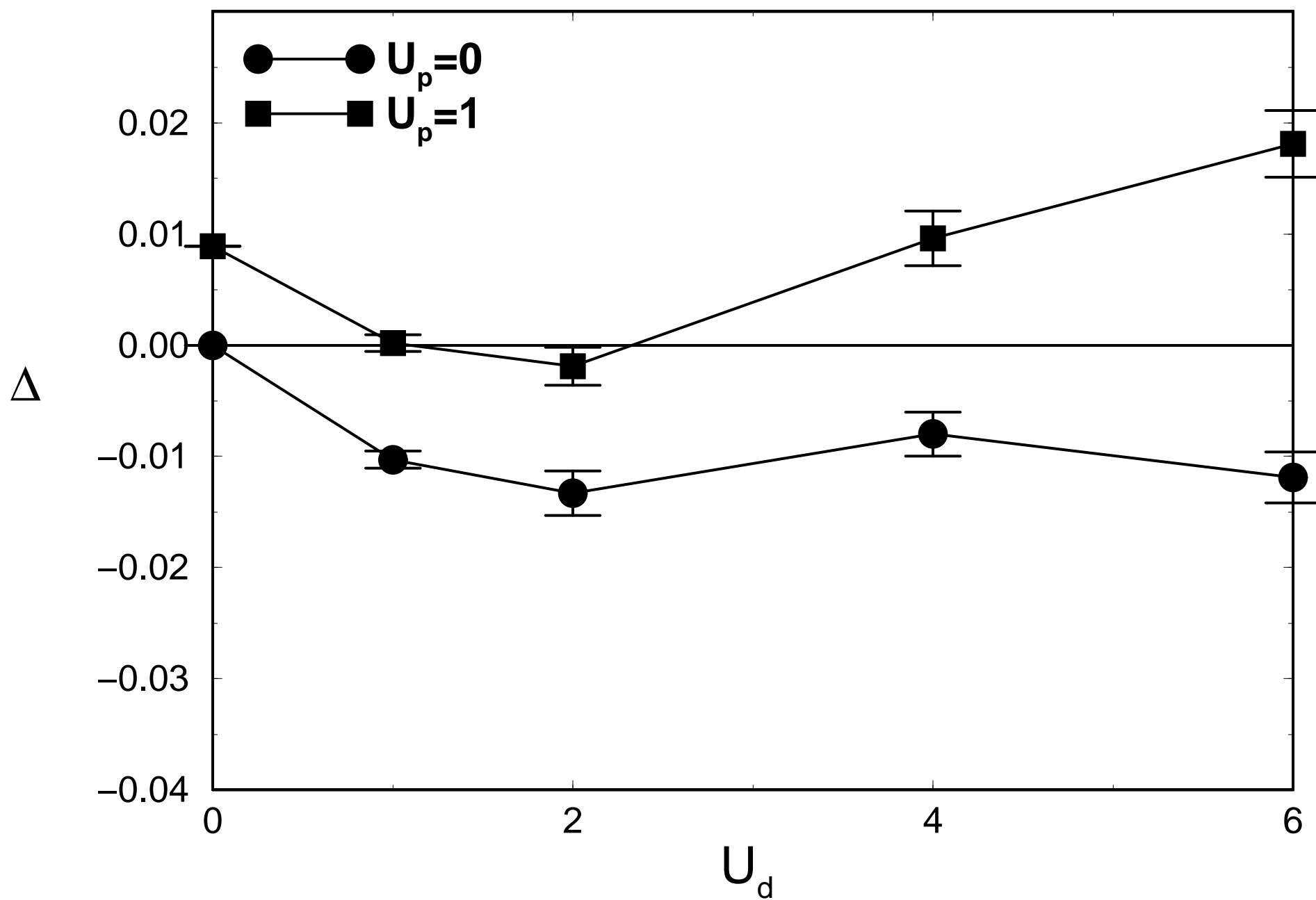


Figure 6b

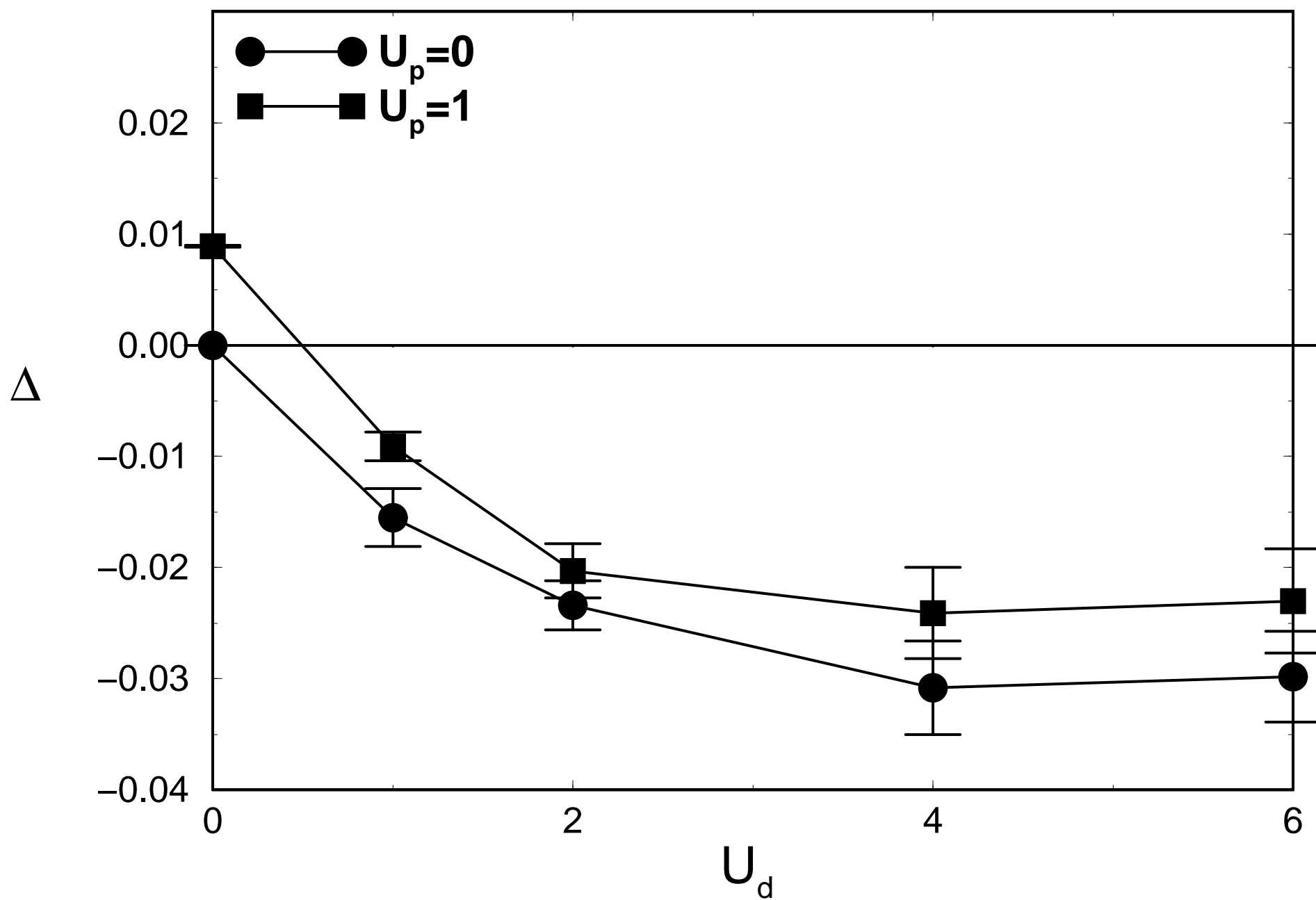


Figure 7

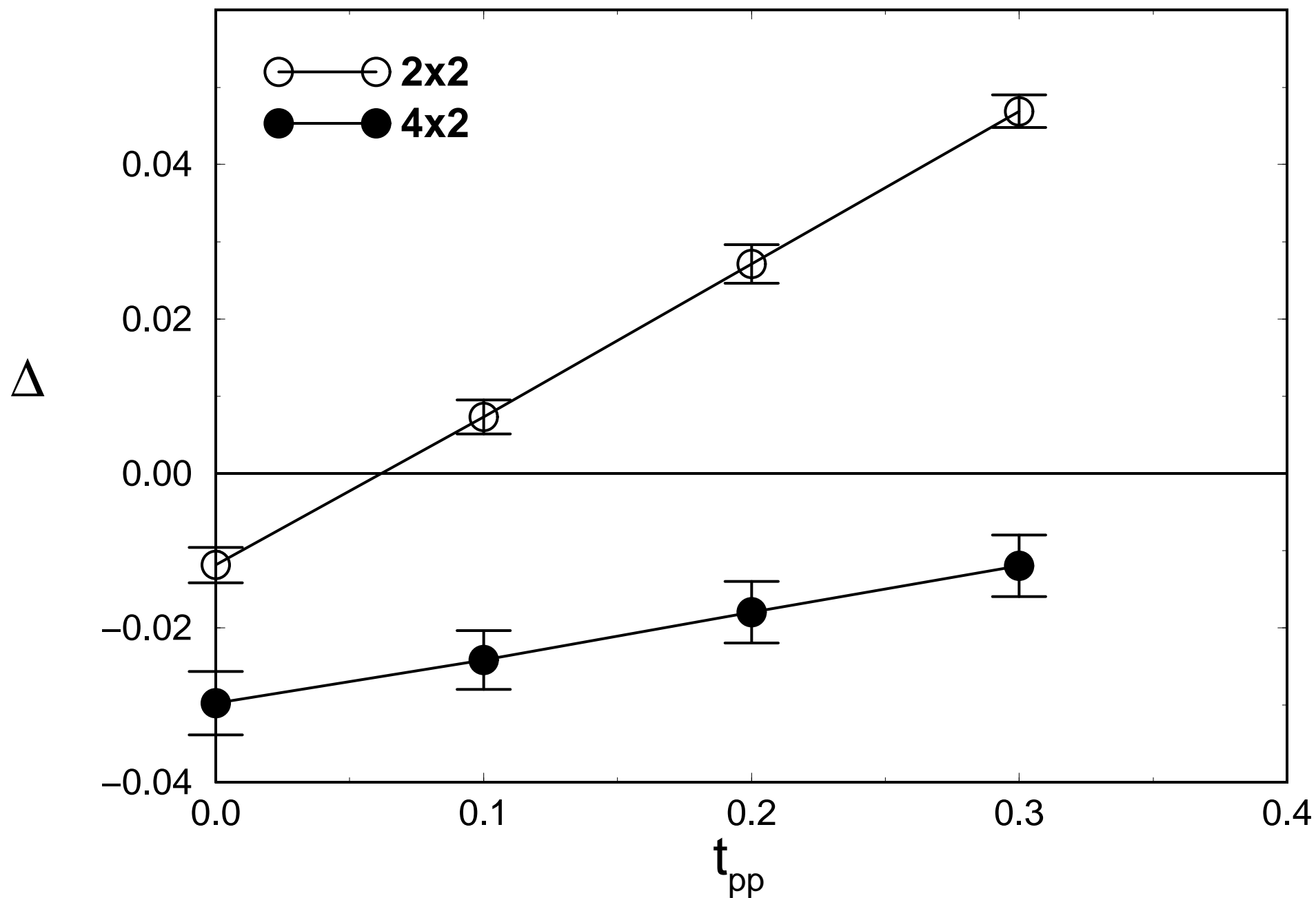


Figure 8

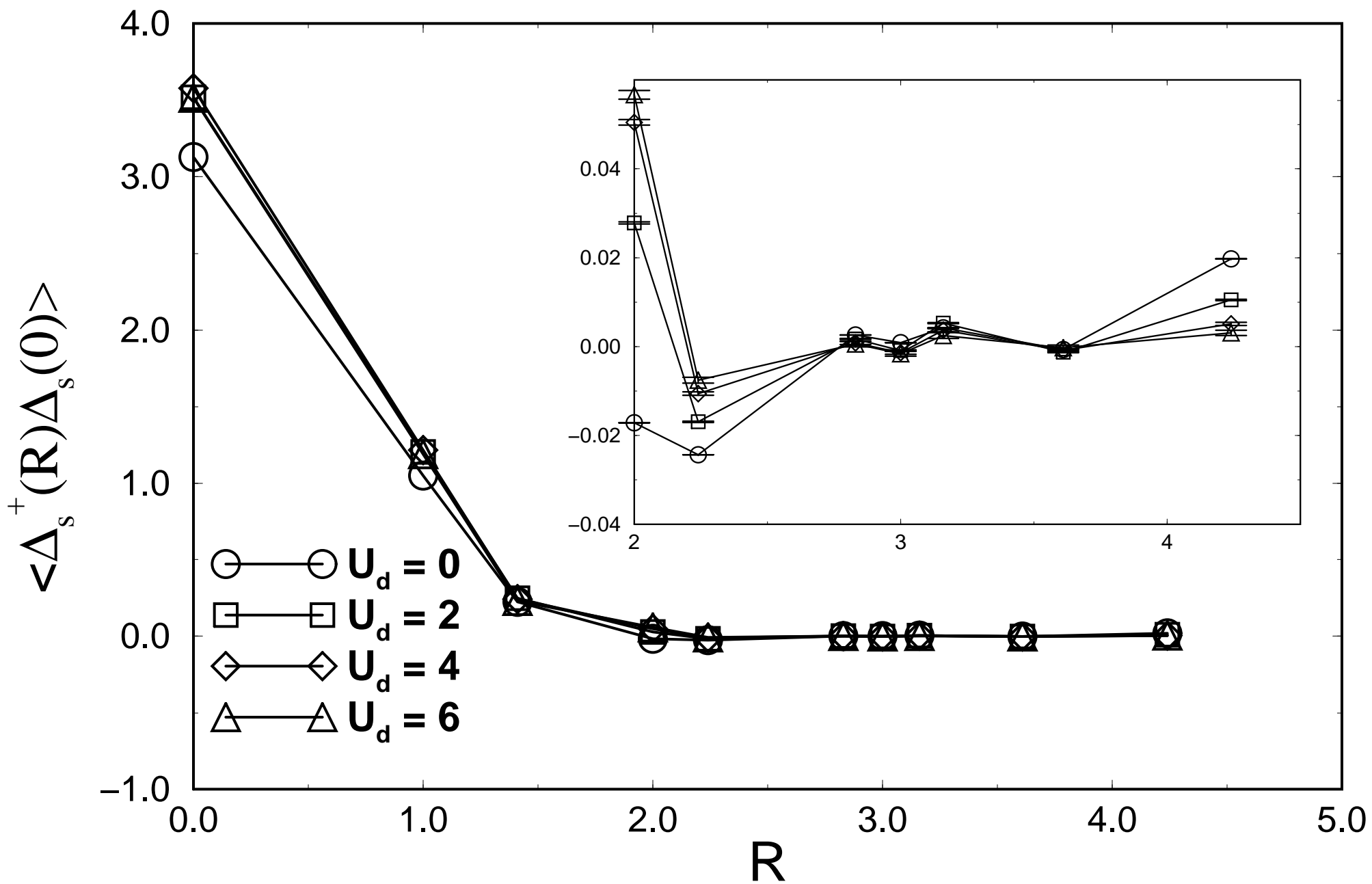


Figure 9

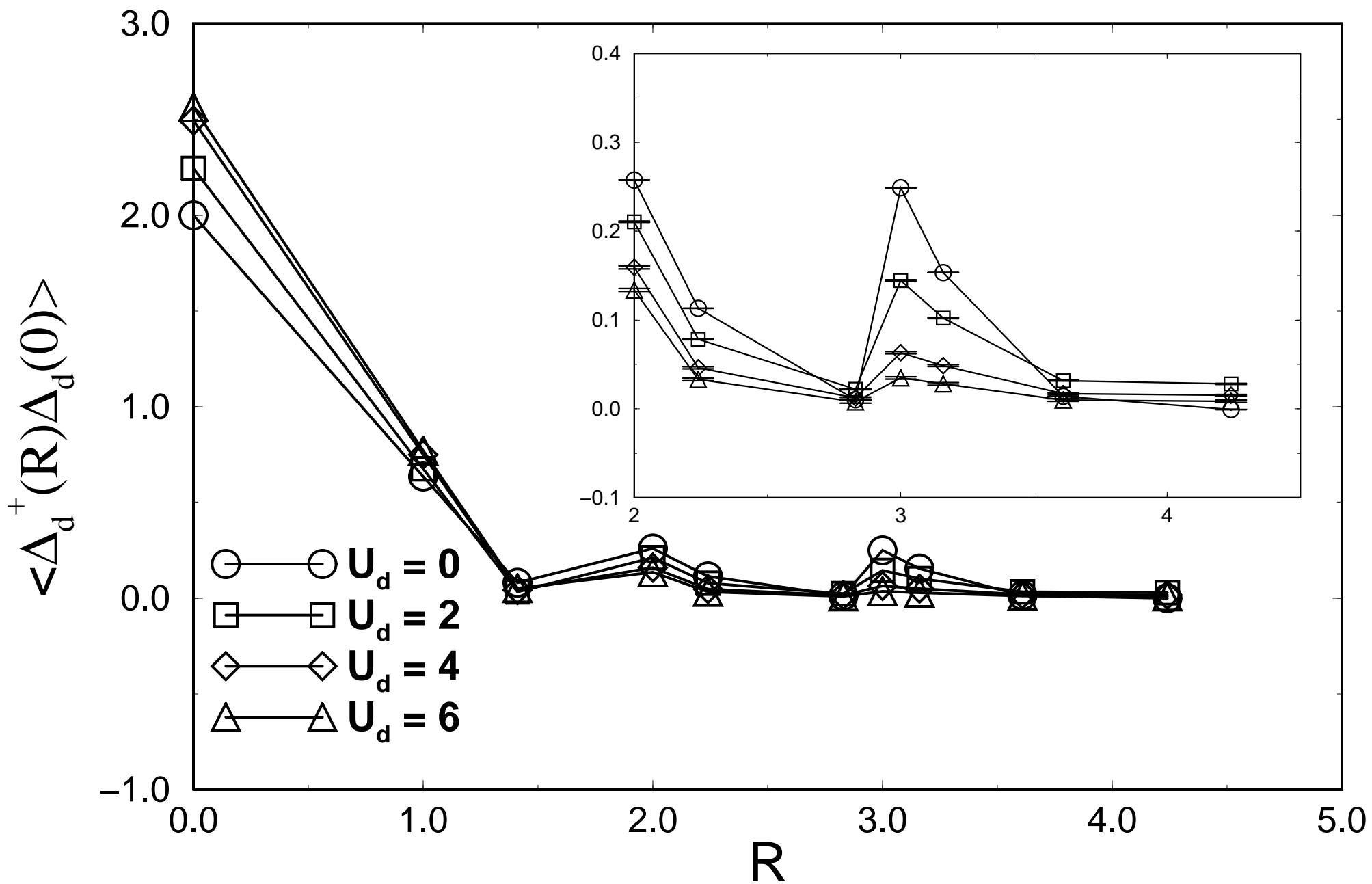


Figure 10

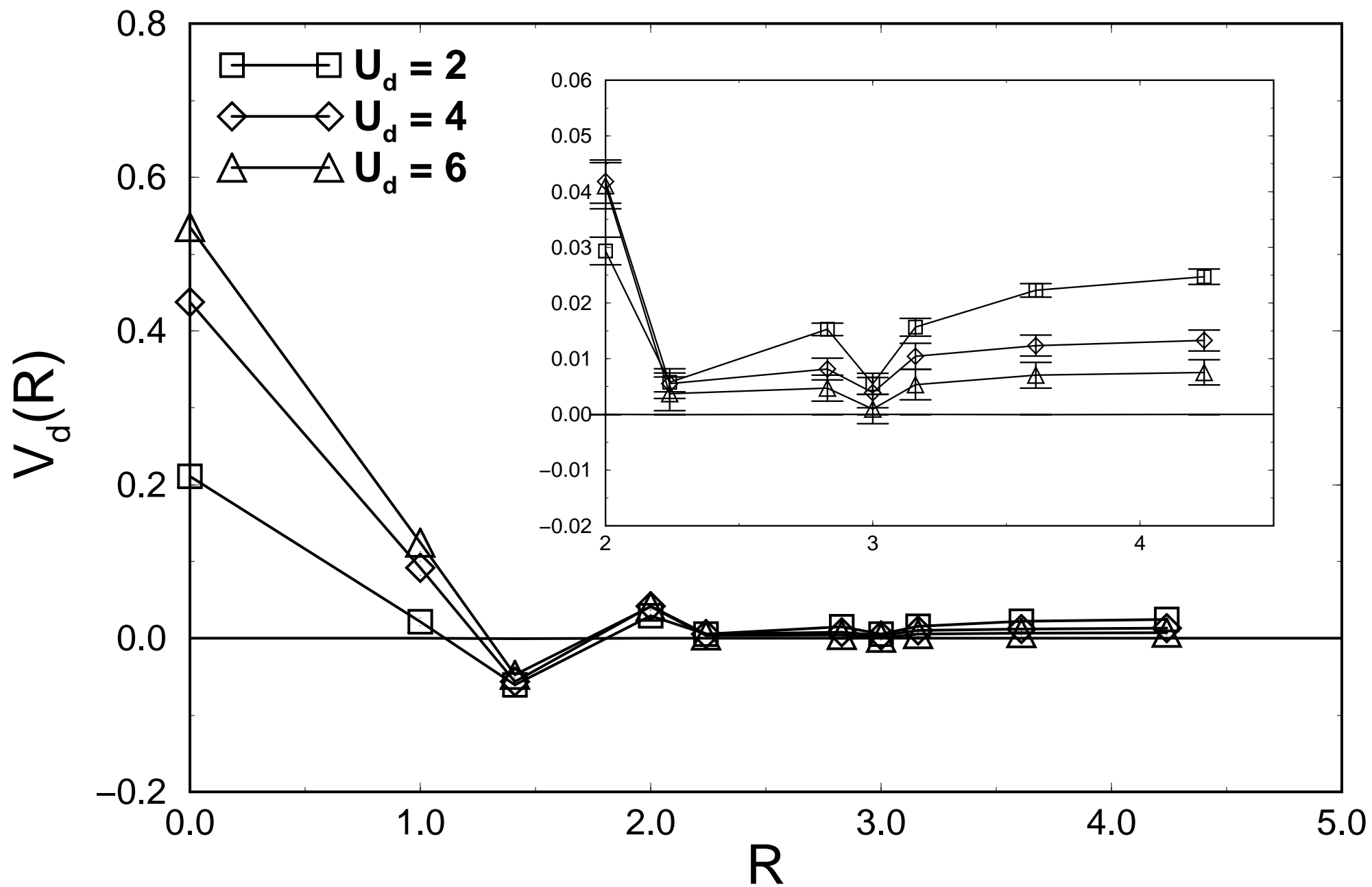


Figure 11

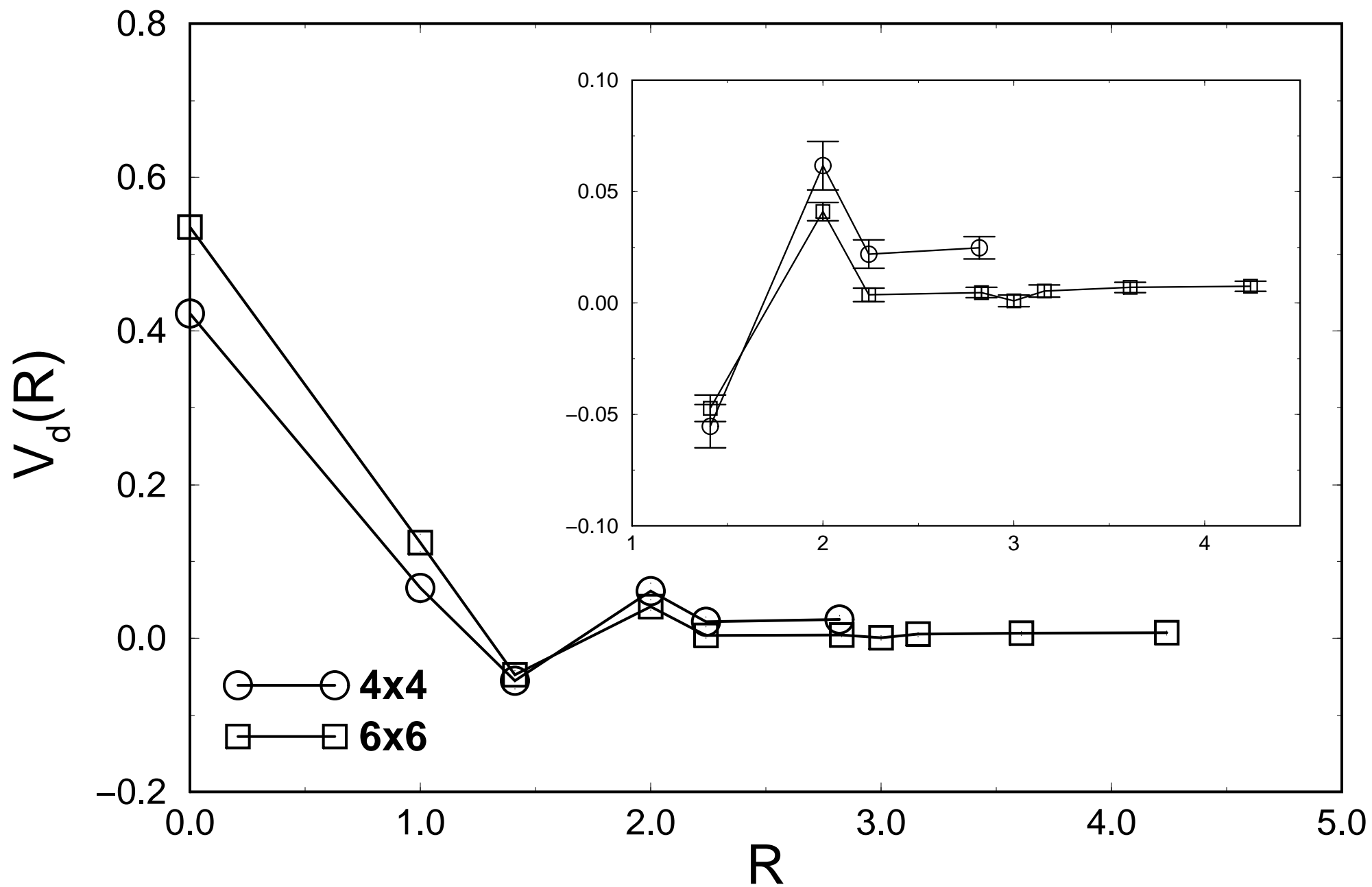


Figure 12

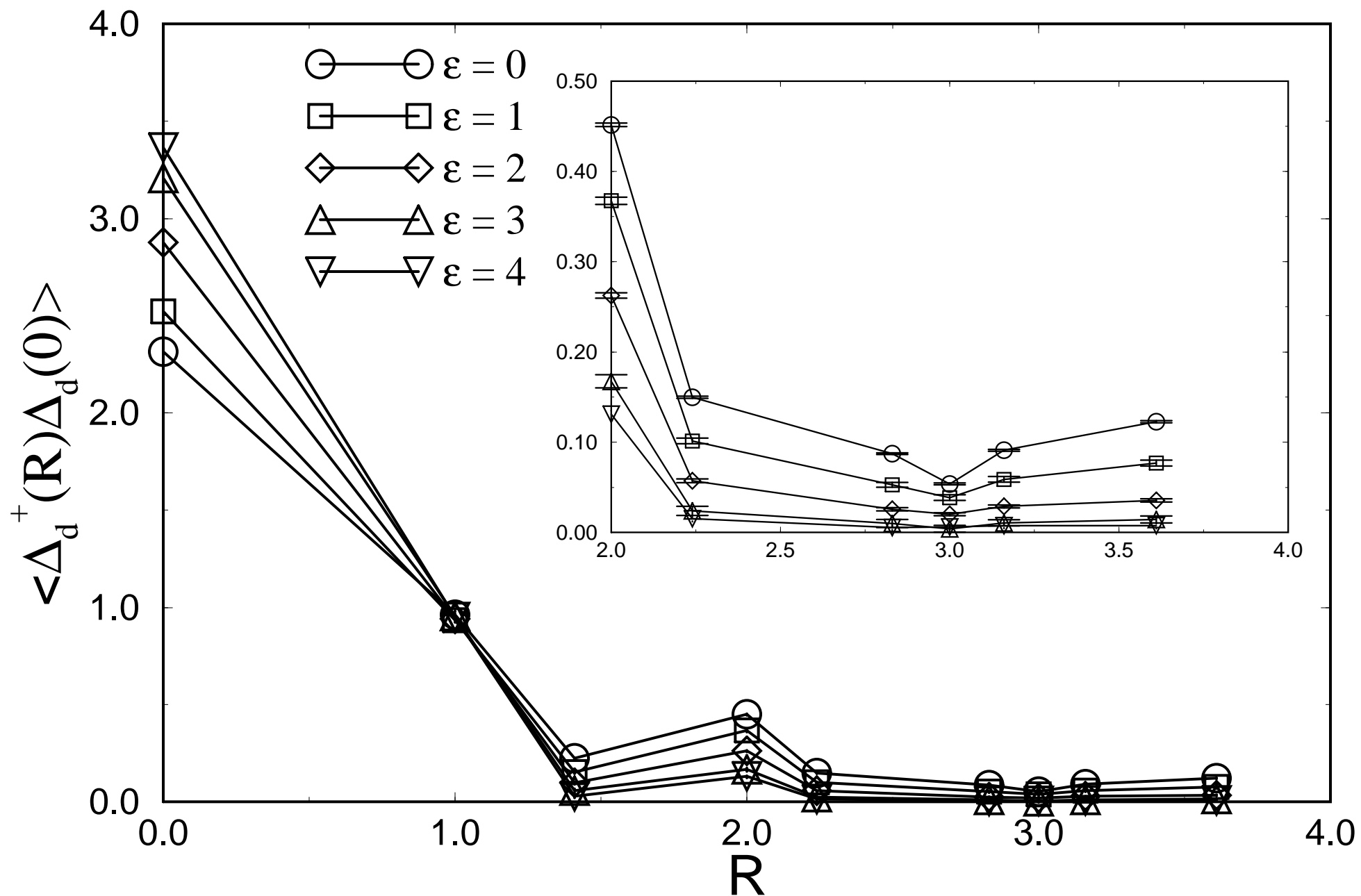


Figure 13

